The Company of **Biologists**

RESEARCH ARTICLE

Bumblebees display characteristics of active vision during robust obstacle avoidance flight

Sridhar Ravi[1,2,*], Tim Siesenop[1], Olivier J. Bertrand[1], Liang Li[3,4,5], Charlotte Doussot[1], Alex Fisher[6], William H. Warren[7] and Martin Egelhaaf[1]

ABSTRACT

Insects are remarkable flyers and capable of navigating through highly cluttered environments. We tracked the head and thorax of bumblebees freely flying in a tunnel containing vertically oriented obstacles to uncover the sensorimotor strategies used for obstacle detection and collision avoidance. Bumblebees presented all the characteristics of active vision during flight by stabilizing their head relative to the external environment and maintained close alignment between their gaze and flightpath. Head stabilization increased motion contrast of nearby features against the background to enable obstacle detection. As bees approached obstacles, they appeared to modulate avoidance responses based on the relative retinal expansion velocity (RREV) of obstacles and their maximum evasion acceleration was linearly related to $RREV_{max}$. Finally, bees prevented collisions through rapid roll manoeuvres implemented by their thorax. Overall, the combination of visuo-motor strategies of bumblebees highlights elegant solutions developed by insects for visually guided flight through cluttered environments.

KEY WORDS: Collision avoidance, Flight control, Insect flight, Neuroethology, Obstacle detection, Spatial vision

INTRODUCTION

The natural habitat of nearly all volant insects is complex. During flight, insects are likely to encounter a myriad of obstacles of varying size, shape and orientation. The ability to anticipate collisions coupled with efficient steering is indispensable for sustainable aerial locomotion. Despite constraints imposed by miniaturization and adverse effects of damage to the wing and the body from in-flight collisions (Foster and Cartar, 2011), insects have evolved to become exceptional flyers, capable of flying long distances through highly complex natural and artificial domains. Insects possess a robust sensorimotor system that enables flight; while their head contains all the sensory apparatus necessary for visual perception, their thorax houses the motor machinery to drive the wings and implement flight manoeuvres (Dudley, 2002). Spatial clutter poses unique challenges to both the sensory and motor systems because obstacles on a collision course need to be extracted parsimoniously with minimal computational latency, while efficient manoeuvres need to be implemented to avoid crashes.

Several previous studies have shown that insects process the motion of images on the retina, i.e. the optic flow, for performing several behaviourally relevant tasks including flight stabilization, visual odometry and course correction during navigation (see Mauss and Borst, 2020; Srinivasan, 2020). Though insects possess two compound eyes, the small spacing between them (Nityananda and Read, 2017) renders stereopsis unsuitable for spatial localization during flight. However, recent research has revealed that insects employ alternative mechanisms to gain spatial information: they use optic flow, which is shaped by active flight and vision strategies so that it can be processed in a computationally parsimonious way (Cellini and Mongeau, 2020; Egelhaaf et al., 2014). Accordingly, insects are thought to shape their aerial trajectory and steady their gaze by condensing head yaw rotations to short periods, saccades, to maximize segments containing high translatory optic flow that is sensitive to the spatial profile of the surroundings (Egelhaaf et al., 2012). Despite the theoretical implications of the previously described saccadic-flight-and-gaze strategy, such as increased saliency of spatial features arising from discontinuities in optic flow, the role of these or other strategies in dealing with spatial complexity such as clutter remains unclear.

Few studies have probed sensorimotor control of insect flight in clutter (Lecoeur et al., 2019), although there exist several supposedly bio-mimetic and insect-inspired collision-avoidance models in the literature. These models mainly use optic flow and classical visual cues such as the retinal size of stimuli and the rate of variation of the stimuli (looming) to guide navigation of an artificial agent (Bertrand et al., 2015; Serres and Ruffier, 2017). The significance of these optical cues for performing visually guided flight behaviours, such as escaping and landing, have been tested in insects (for review, see Fotowat and Gabbiani, 2011; Baird et al., 2013; van Breugel and Dickinson, 2012). However, there is little behavioural evidence on the visual variables that may be used to guide flying insects through cluttered environments. From a sensory standpoint, it will be useful to identify strategies that enable flying insects to extract relevant features of their surroundings, such as obstacles and gaps, and the cues they use to modulate collision-avoidance responses. From a motor control standpoint, recent studies have highlighted the flight behaviour of insects around static and moving obstacles (Burnett et al., 2020; Mountcastle et al., 2016) and the biomechanics of the evasive manoeuvres orchestrated to achieve energetically sustainable flight around obstacles forms an important component of our understanding of insect locomotion through natural habitats.

Bumblebees are excellent fliers and frequently navigate through dense vegetation while foraging or returning to their nest. Much is known about both the flight and navigational performance of

[1]Department of Neurobiology and Center of Excellence Cognitive Interaction Technology (CITEC), Bielefeld University, 33619 Bielefeld, Germany. [2]School of Engineering and Information Technology, University of New South Wales, Canberra, ACT 2600, Australia. [3]Department of Collective Behavior, Max Planck Institute of Animal Behavior, University of Konstanz, 78464 Konstanz, Germany. [4]Centre for the Advanced Study of Collective Behaviour, University of Konstanz, 78464 Konstanz, Germany. [5]Department of Biology, University of Konstanz, 78464 Konstanz, Germany. [6]School of Engineering, RMIT University, Melbourne, VIC 3001, Australia. [7]Department of Cognitive, Linguistic & Psychological Sciences, Brown University, Providence, RI 02912, USA.

*Author for correspondence (sridhar.ravi@adfa.edu.au)

S.R., 0000-0001-7397-9713; O.J.B., 0000-0002-0889-4550

bumblebees (Baird and Dacke, 2012; Crall et al., 2015; Osborne et al., 2008), thus making them an excellent model organism to analyse how flight motor and vision systems combine to enable flight through complex spatial environments. Here, after bumblebees were trained to fly freely in an unobstructed tunnel, we presented them with several unfamiliar obstacles that they had to negotiate while en route to their hive. The instantaneous position and orientation of the bumblebees' head and thorax were tracked as they approached and evaded obstacles to understand the in-flight dynamical relationship between these two morphological body segments and examine the possible role of active vision strategies. Optic flow experienced by the bees was reconstructed and analysed to identify properties of their sensorimotor system that may facilitate obstacle detection and salient visual cues that may be used to steer collision avoidance. Finally, flight dynamics of the bees as they avoided collisions was analysed to uncover the motor inputs of their evasive manoeuvres.

MATERIALS AND METHODS
Experiment setup and procedure

Experiments were conducted with individuals from a *Bombus terrestris* (Linnaeus 1758) colony that was maintained within the lab at room temperature (22°C), with large windows that let natural light into the room. A healthy hive sourced from a commercial breeder (Koppert Biological Systems) was placed within a 0.5×0.5.0.3 m mesh enclosure that was covered with dark cloth to simulate the natural underground habitat of the bees (Movie 1). The hive enclosure was connected to a 0.20×0.25×1.5 m flight tunnel that led to a 1×1×0.75 m foraging chamber where gravity feeders containing 30% (w/w) sucrose solution blended with 1% commercial honey were placed. The side walls and floor of the tunnel were lined with a random cloud pattern with spatial frequencies varying by $1/f$, similar to that used in Ravi et al. (2019). The ceiling of the flight tunnel consisted of 5 mm transparent acrylic panels that spanned the width of the tunnel. Connections between the hive enclosure, flight tunnel and foraging chamber were made using 30 mm internal diameter and 150 mm long flexible silicon tubing. The bees and hive were given 1 week for habituation to the environment before experiments.

Fifteen foraging bumblebees of similar size were selected for flight experiments. As some bees flying within the flight tunnel tended to meander and perform exploration-type flights, only bees that made fast direct flights within the tunnel were recruited for experiments. The bees were captured as they returned from the foraging chamber to the hive and cold anaesthetized by leaving them in a refrigerator at 4°C for 6–10 min (until no movement was visibly detected). Once they were immobile, a triangular marker was affixed to the dorsal surface of the thorax using cyanoacrylate glue (super glue, UHU). The marker consisted of three white spheres (0.2 mm diameter) representing the vertices of an isosceles triangle (measuring 2.7×2.3 mm) set upon a black background (Fig. 1; Movies 1 and 2); markers were identical to those used in Doussot et al. (2021) and Odenthal et al. (2021). Footage of the bees in flight revealed that the marker had a sufficient distance from the wings and did not interfere with wing kinematics. Working under a binocular microscope, three additional markers consisting of water-soluble white and non-toxic white paint [Hobbyline, Matt Fabre (Acryl)] were also carefully placed on the head, ensuring that the ocelli were not occluded by the markers. The marked bee was then placed in a transparent chamber at room temperature and ambient lighting and allowed to recover, which occurred within 15 min.

Prior to the experiments, gates on either side of the flight tunnel were closed to prevent bees from entering the tunnel. During experiments, blinds over the windows were drawn and a 1000 W halogen floodlight with a large diffuser in front created homogeneous lighting; this setup was similar to that described in Ravi et al. (2019). The roof was momentarily removed and an obstacle course consisting of 8 vertical cylinders (7 mm diameter and 250 mm height) was then placed within the tunnel (see Fig. 1A). All vertical cylinders (obstacles) were attached at the bottom to a 5 mm grey PVC platform for easy placement and retrieval from the flight tunnel. Obstacles were placed along four longitudinal stations separated by 75 mm while the obstacles at each station were laterally separated by 70 mm (see Fig. 1A; Movie 1). This arrangement was chosen to elicit manoeuvring flight from the bees. Markings on the flight tunnel floor ensured consistency in positioning the obstacle course within the tunnel.
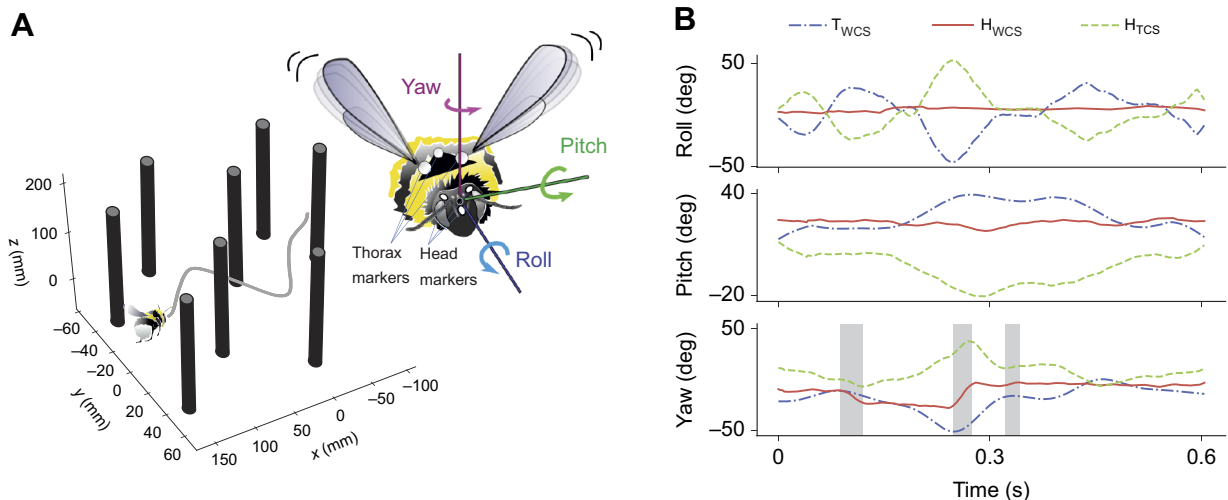

Fig. 1. Experimental setup and sample flight data. (A) Schematic diagram of the flight tunnel with a sample flight trajectory of a bee through the obstacle tunnel; note that the scale of the *x*- and *y*-axes differs. Inset shows the markers on the bee's head and thorax as well as the yaw, pitch and roll axes. (B) The time-resolved roll, pitch and yaw orientation of the bee's thorax (T) and head (H) in the world coordinate system (WCS) for the flight shown in A. Also plotted is the orientation of the head relative to the thorax, i.e. based on the thorax coordinate system (TCS). Grey shaded regions in the time course of the yaw angle indicate head saccades, while the intersaccade segments of the flight are unshaded.

Experiments were performed on one bee at a time. Once a marked bee had fully recovered and was flying freely with the markers intact, it was placed in the foraging chamber. The bee became airborne upon release within the foraging chamber and after a few minutes it steadily approached the gateway to the flight tunnel. The gate was then opened, and the bee flew through the flight tunnel while slaloming past the obstacles on its way back to the hive (Movies 1 and 2). To ensure we captured the response of naive bees dealing with a complex environment, the obstacle course was retrieved from the flight tunnel once the marked bee returned to the hive. All gates were subsequently opened to all general foraging traffic. This process was repeated for 15 marked bees and only their first flight through the obstacle course was considered for analysis.

Position and orientation estimation

Three Optronis CR3000×2 high-speed cameras were placed above the obstacle course: two of the cameras bilaterally overlooked the tunnel at approximately 30 deg from the vertical and the third camera was positioned longitudinally around 45 deg from the vertical. The flights of the bees were recorded at 500 Hz with a shutter of 1/2000 s, and the region approximately covering 180×180×200 mm (length×width×depth) was kept in focus. During post-processing, lens distortion was corrected by using standard MATLAB Image Processing Toolbox routines. A conspicuously marked object of known dimensions was placed within the field of view at mid-height of the tunnel and volume of interest was calibrated using the open-source MATLAB-based routine DLTdv5 (Hedrick, 2008). The same package was used to digitize the recorded flight sequences. A total of six points (three points on the head and three on the thorax) were digitized for each of the 15 bees. During the entire flight, each marker was made up of only 7–10 pixels; therefore, the digitization error in localizing the centroids of marker points on the thorax was estimated to be much smaller (<2 pixels) than the mean number of pixels separating the markers (~50). This localization error can be expected to be higher for the head, as the markers were smaller and more closely spaced; therefore, utmost care was taken during digitization, which was performed manually for most segments of the flight. To remove higher-frequency errors due to the digitization process, position data of all markers were passed through a 4th-order, low-pass Butterworth filter with a cut-off frequency of 100 Hz, which is lower than the Nyquist frequency (250 Hz) but significantly higher than the genuine frequencies of the manoeuvres performed by the bees. The accuracy of the 3D localization was assessed by measuring the variation in the absolute distance between each point of the triangles on the head and thorax; the distances between the marker points are known and constant as they were located on a rigid substrate. Only cases where the variation was <3% compared with the median were considered for analysis, similar to the process followed in Doussot et al. (2021) and Ravi et al. (2016).

Instantaneous velocities and accelerations of the head and thorax of the bees were calculated by first estimating the centroid of the markers of the head and thorax, respectively, and taking their time derivatives. Translational accelerations of the head and thorax were calculated in both a local and a global coordinate system that was attached to the flight tunnel (the longitudinal axis was aligned with the long axis of the flight tunnel; the lateral and vertical axes span the cross-section in the horizontal and vertical directions, respectively). To reconstruct the head and thorax orientation, we defined three coordinate systems: the reference frame of (1) the head-centred coordinate system (HCS) and (2) the thorax-centred coordinate system (TCS) as defined by the head or thorax markers,

respectively, and (3) the world coordinate system (WCS) attached to the flight arena (Fig. 1). Assuming rigid thorax dynamics, the instantaneous orientation and rotation rates of the HCS and TCS planes were calculated with respect to the WCS following the roll–pitch–yaw Euler notation. This method has been extensively used in several studies involving insect flight (e.g. Ravi et al., 2016) and is identical to that described in other studies (e.g. Doussot et al., 2021). Saccades were identified using the two-threshold method similar to Doussot et al. (2021) and Riabinina et al. (2014) where the yaw rate of the head was temporally filtered using a threshold at 260 deg s^{-1} and data points were considered part of the same saccade if rotation rate was greater than 170 deg s^{-1}. Saccade duration was estimated by measuring the temporal distance between the instance the yaw rate began increasing due to the saccade to the instance the yaw rate returned to zero after passing through the peak. On average, each bee performed three saccades as they flew through the region being recorded by the high-speed cameras, and a total of 53 saccades were identified from all 15 flights.

Optic flow estimation

Geometric optic flow measured as the angular displacement of the vector between an arbitrary point in space and the retina due to relative motion was calculated in MATLAB using the digitized coordinates and flight tunnel geometry including the obstacles. Here, for each instance of the flight, the true geometric optic flow was calculated assuming a spherical compound eye and the retina approximated as a point, similar what has been described previously (Ravi et al., 2019) (see Movie 3). The geometric optic flow was calculated by first discretizing the ommatidium as a ray emanating from the point retina. The compound eye was considered to consist of 181×181 rays equally spaced along the elevation and azimuth of the spherical eye; thus, the inter-ray angle along the elevation and azimuth was 1 deg and 2 deg, respectively. Further details on the sequence of computations to evaluate the true optic flow have been presented previously (Ravi et al., 2019), and the method is also similar to the ray-casting method implemented in numerous previous studies (Bertrand et al., 2015; Lecoeur et al., 2019; Shoemaker et al., 2011). For each time step, the optic flow calculations provided vector fields that included both magnitude and the azimuthal and elevation components of the optic flow for each ommatidium.

The nearness map, defined as the inverse of the absolute distance between the retina and features in the environment, was also created for each time step (see Movie 3). This was calculated by taking the inverse of the absolute magnitude of the ommatidium ray that connected the retina and the respective solid point in the environment (Bertrand et al., 2015). For pure translation motion, the optic flow is lower for objects further away than for nearer ones; therefore, a positive correlation is expected between the nearness map and optic flow. Thus, the strength of the correlation provides a measure of the extent to which the optic flow can be considered as representative for the actual relative spatial layout of the environment.

Collision avoidance flight segments

The portion of the trajectory where a bee avoided an imminent collision was isolated and the intersaccade region within this portion was analysed. As the obstacles were placed in pairs along longitudinal stations in the flight tunnel (Fig. 1; Movies 1 and 2), for each instance, only the pair of obstacles immediately ahead of the bee was considered. This was reasonable because all bees steadily progressed through the tunnel and did not seem to be

affected by the obstacles behind them. The bee was then approximated as a sphere of 30 mm diameter and for each instant, the sphere was linearly translated in the x–y plane along the instantaneous velocity vector of the bee, to test whether it intersected either of the two obstacles (represented as a circle) that were immediately ahead of them. Segments of flights where a bee was clearly on a collision course with an obstacle were isolated by first trimming the total trajectory to regions between consecutive longitudinal stations of obstacles (see Fig. 1A). Flight segments between two longitudinal stations were considered for analysis only if the trajectory of the sphere along the instantaneous velocity vector of the bee intercepted one of the two obstacles for greater than 30% of the flight segment. Though this limit was arbitrarily chosen, the results did not vary significantly with small changes to this threshold. Based on this method, those cases where an imminent collision was likely to occur were isolated while those trajectories where the bees flew between obstacles or may have momentarily tended towards one of the obstacles were not considered. Through this method, 40 flight segments where imminent collisions were averted were identified and analysed.

Statistical analysis

A total of 15 flights were recorded and analysed in this study. As the data were collected from individually marked bees, we performed a paired t-test to compare variation in mean parameters within the same individuals of the population, such as the mean contrast in optic flow generated by the head and body orientation and trajectory or the difference in mean variation in body versus head orientation, etc. The significance of the slope of the linear regression between parameters was tested using a t-statistic test and the R^2 value was used to indicate goodness of fit. All statistical tests were performed in MATLAB and $P<0.05$ was considered to indicate a statistically significant difference between the quantities being tested. For cases where multiple comparisons were made within each experimental condition, Bonferroni correction was implemented.

RESULTS

Flight trajectory and orientation

On entering the obstacle course, the bumblebees continued to progress along the flight tunnel with a mean flight speed of 0.33 ± 0.09 m s^{-1} while slaloming between obstacles (Fig. 1A; Movie 2) and no collisions were noted in any of the 15 flights that were recorded. Among all flights ($n=15$), the mean variation (s.d.)

of the bees' lateral velocity was highest, while on average the bees minimally varied their longitudinal velocity (Fig. 2A) (longitudinal–lateral and vertical–lateral $P<10^{-4}$ and longitudinal–vertical $P=0.0080$; $n=15$, d.f.=28). This was also reflected in the acceleration of the bees, where across all flights the mean variation in longitudinal and vertical acceleration was similar (Fig. 2B), while the mean variation along the lateral axis was significantly higher (longitudinal–lateral and vertical–lateral $P<10^{-4}$ and longitudinal–vertical $P=0.0615$; $n=15$, d.f.=28).

Markers on the head and thorax of the bees allowed us to analyse and compare the orientation, with respect to the global coordinate system, of both body segments during flight (see Materials and Methods; Fig. 1; Movies 1 and 2). The mean variation in thorax roll was significantly more than pitch or yaw rotations, while on average the pitch variation was lowest (roll–pitch $P<10^{-4}$, yaw–pitch $P=2.86\times10^{-6}$, roll–yaw $P=5.46\times10^{-5}$; $n=15$, d.f.=28) (Fig. 2C). In contrast, the mean variation in head orientation was greatest for yaw, and significantly smaller for both roll and pitch (roll–pitch $P=0.3041$, yaw–pitch and roll–yaw $P<10^{-4}$; $n=15$, d.f.=28) (Fig. 2C). The temporal profile of the bees' head yaw orientation could be separated into saccade and intersaccade segments (see Materials and Methods; Fig. 1B; Movie 2). Across all flights, the mean variation in head yaw during the intersaccade periods (segment of flight between successive saccades; see Fig. 1B) was significantly smaller and statistically similar to the mean roll and pitch variation of the head (yaw–pitch $P=0.6364$, roll–yaw $P=0.498$; $n=15$, d.f.=28) (Fig. 2C). Comparing the magnitude of rotations of the head and thorax revealed that the mean variation in roll and pitch of the bees' thorax was significantly greater than that of the head (roll and pitch $P<10^{-4}$; $n=15$, d.f.=28). Considering the entire flight sequence (including saccades), mean variation in yaw rotations of the head and thorax was not statistically different ($P=0.818$; $n=15$, d.f.=28); however, during intersaccades, mean variation in head yaw rotations was much smaller than that of the thorax ($P<10^{-4}$; $n=15$, d.f.=28) (Fig. 2C). Unlike the head, the yaw profile of the thorax consisted of relatively smooth variation in orientation. Therefore, the time course could not be separated into distinct saccade and intersaccade segments using the same thresholds used to segment the head yaw orientation (see Materials and Methods for saccade extraction process) (Fig. 1B).

The normalized correlation between the time course of the orientation of the bees' head and thorax in the WCS revealed that
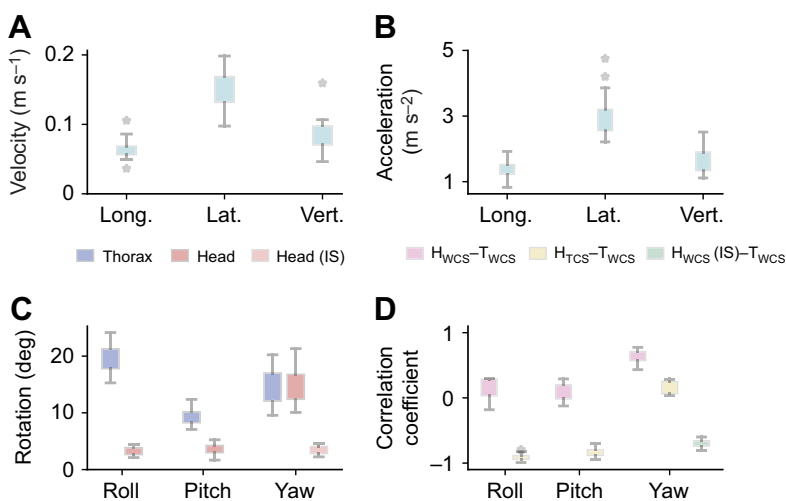

Fig. 2. Flight parameters and orientation of head and thorax. (A,B) Standard deviation of the time-dependent fluctuations in bee head velocity (A) and acceleration (B), based on the WCS. All velocities and accelerations were measured from the centroid of markers on the head. (C) Standard deviation of the roll, pitch and yaw rotations of the thorax and head in the WCS. Variation in yaw rotation of the head for intersaccade sections (IS) alone is also included. (D) Normalized correlation between the time course of the roll, pitch and yaw orientation of the head in the WCS and TCS, and of the thorax in the WCS for bees during the entire flight. Also included is the normalized correlation between the time course of the bees' thorax and head yaw in the WCS only for the intersaccade (IS) segments of the flight. $n=15$ for all parameters in A–D.
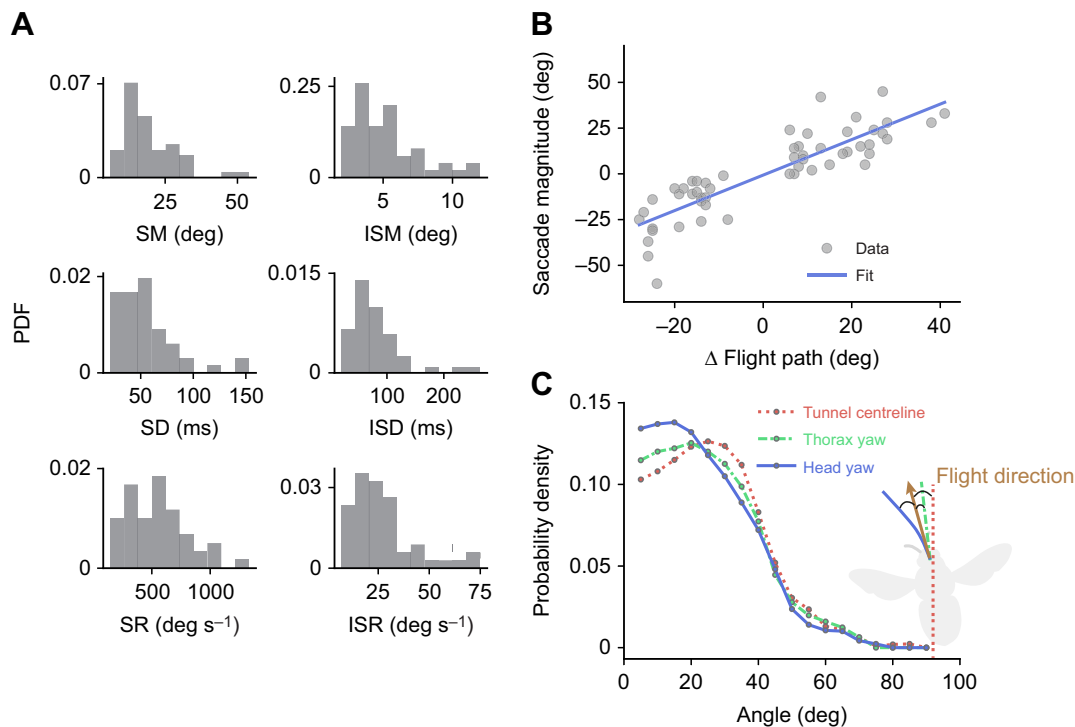
Fig. 3. Saccades and flight path. (A) The probability density function (PDF) of different properties of the bees' head saccades (n=54) and intersaccades (n=66) for all flights. SM, saccade magnitude; ISM, intersaccade magnitude; SD, saccade duration; ISD, intersaccade duration; SR, saccade rate; ISR, intersaccade rate. (B) Scatter plot of the magnitude of saccade yaw of the head during a saccade versus the magnitude of variation in the flight direction of the bees before and after the saccade (n=54, fit equation y=0.969x−0.67, R^2=0.749, slope P=1.95×10^{-17}). (C) PDF of the angle between the instantaneous values of the bees' flight direction and the centreline of the tunnel, thorax yaw and head yaw for all flights.

thorax roll and pitch rotations were nominally uncorrelated with those of the head (Fig. 2D). However, the time course of the yaw orientation of the head and thorax was positively correlated and significantly higher (roll–pitch P=0.475, yaw–pitch and roll–yaw $P<10^{-4}$; n=15, d.f.=28) (Fig. 2D). But, if only the intersaccade segments were considered, the yaw rotations between the head and thorax were uncorrelated and on average across the different flights did not differ statistically from those of roll and pitch (intersaccade yaw–pitch P=0.134, intersaccade yaw–roll P=0.625; n=15, d.f.=28). Comparing the time course of the head orientation of the bees in TCS and the thorax orientation in the WCS can provide some insight into the extent of coordination between these two body segments. A strong negative correlation was noted between the head (TCS) and thorax (WCS) in roll and pitch while a relatively lower but also negative correlation was noted for yaw (Fig. 2D).

Saccades and flight path

Across all recorded flights, the mean (±s.d.) and maximum rotation rate of the bees' head yaw during a saccade was 620±245 deg s^{-1} and 1300 deg s^{-1}, respectively (Fig. 3A). As the bees negotiated the obstacles, saccades lasted around 51±29 ms (median±s.d.) and the median variation in the head yaw angle during the saccade was 17±10 deg. In contrast, intersaccades lasted on average 86±47 ms (median±s.d.) where the median (±s.d.) yaw variation was 6±3 deg and the mean (±s.d.) head rotation rate was 30±16 deg s^{-1} (Fig. 3A). The relationship between the saccades and the bees' flight direction was explored by comparing the change in direction of the bees' flight path (measured from the centroid of the markers on the head) before and after a saccade with the magnitude of the saccade. A strong linear relationship was noted (n=54, R^2=0.81, regression slope=0.969) between the change in head yaw angle during a

saccade and the change in the direction of the flight trajectory (see Fig. 3B).

To further examine the relationship between the bees' flight profile and orientation of their head and thorax, for all flights, the probability density function of the angular offset between the instantaneous flight direction of the bees (calculated from the centroid of the head markers) and the centreline of the flight tunnel, the yaw angle of the thorax and the yaw angle of the head was estimated (see Fig. 3C). As expected, the bees' flight direction deviated considerably from the centreline of the tunnel as they navigated between obstacles (Fig. 3C). Similarly, the bees' flight direction deviated considerably from the yaw angle of their thorax, with nearly 30 deg of deviation (sideslip) occurring for over 60% of the flight duration. However, as compared with the thorax, the head was most aligned with respect to the flight trajectory, with deviations of >20 deg occurring for only <15% of the flight duration (Fig. 3C).

Optic flow analysis

To quantify the effects of the in-flight orientation of the bees' head and thorax on visual information, the instantaneous optic flow was separately computed using the time course of the flight trajectory and orientation of the head and thorax, respectively (Fig. 4A,B). Not only were obstacles more discernible in the optic flow computed using head position and orientation (Fig. 4B; Movie 3) but also the overall profile of optic flow across the visual field more closely matched the nearness map (Fig. 4C; Movie 3). As expected, during saccades the optic flow across the visual field was dominated by head rotation (see Fig. 4D). The optic flow contrast of the obstacles with respect to their background during intersaccades was estimated similar to the process followed in Ravi et al. (2019). The optic flow contrast was defined as the difference between the optic flow over
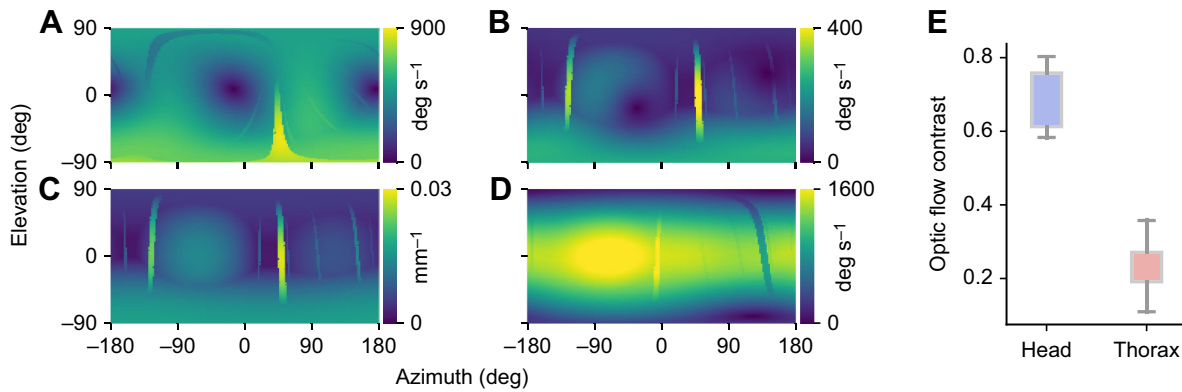
Fig. 4. Sample snapshot of the total geometric optic flow for a full spherical field of view at a given instant during flight. (A,B) Optic flow was calculated using (A) thorax and (B) head trajectories and orientation. (C) Snapshot of the nearness map for the head trajectory and orientation for the same instant as that shown in A and B. The optic flow generated from the head data (B) bears a very close resemblance to the nearness map that represents the true geometric profile of the environment (C). The obstacles are also clearly identifiable in the optic flow generated from the head rather than from the thorax data (A). (D) Snapshot of the optic flow from the head trajectory and orientation during a saccade from the same flight as that shown in A–C. The large yaw rotations of the head dominate the optic flow profile. (E) Mean contrast in optic flow resulting from the nearest obstacles versus the background optic flow for all flights (n=15, head–thorax $P<10^{-4}$). Optic flow contrast estimated in the frontal region of the gaze (azimuth: −90 deg to 90 deg, elevation: −60 deg to 60 deg).

the obstacle and that of the background, measured along a line that was 6 deg outside and parallel to the edge of the obstacle; this difference was then divided by the background flow rate. The contrast was also significantly higher for the optic flow generated by the head as compared with the flow generated using thorax data (head–thorax $P<10^{-4}$) (Fig. 4E).

Obstacle approach and flight-path deviation

For all recorded flights, the portion of trajectory was isolated where the bees encountered an obstacle in their flight path and then deviated to avoid an imminent collision. The intersaccade segments within these isolated trajectories was considered for analysis (see Materials and Methods: Figs 5 and 6A). To uncover possible cues that may be used by the bees for navigating between the obstacles, three classically considered visual parameters (Fotowat and Gabbiani, 2011), including retinal size (γ, see Eqn 1), rate of change of retinal size ($\dot{\gamma}$, see Eqn 2) and relative retinal expansion velocity (RREV; Wagner, 1982; see Eqn 3), were evaluated for each instant of the flight segments and compared with the time course of the bees' acceleration:

$$\gamma(t) = 2\sin^{-1}\frac{r}{d(t)}, \tag{1}$$

$$\dot{\gamma}(t) = \frac{d\gamma}{dt}, \tag{2}$$

$$\mathrm{RREV}(t) = \frac{\dot{\gamma}(t)}{\gamma(t)}, \tag{3}$$

where γ is the angle subtended by the obstacle on the bees' retina along the x–y plane. As the obstacle was a circular cylinder, γ is the angle between two vectors that are tangential to the circle (obstacle cross-section) and intersect at the bees' retina. r is the radius of the obstacle, d is the distance between the centre of the bees' eye and the centre of the obstacle, $\dot{\gamma}$ is the rate of optical expansion of the obstacle and t is time.

As expected, γ increased as the bees approached the obstacle until it reached a maximum followed by a reduction, signifying an increase in the relative distance between the object and the bee (see Figs 5 and 6B). Similarly, $\dot{\gamma}$ also increased and then steadily

decreased as the bees approached and deviated from the obstacles. Both the maximum retinal size of the obstacle (γ_{max}) and the maximum rate of expansion of the obstacles ($\dot{\gamma}_{max}$), for all flight segments, had a poor but positive linear regression slope with the acceleration of the bees at that instant (see Fig. 7A,B). The RREV also tended to increase as the bees approached an obstacle, reaching a maximum followed by a decrease (Fig. 5). For all trajectories, maximum RREV (RREV$_{max}$) occurred during the approach and
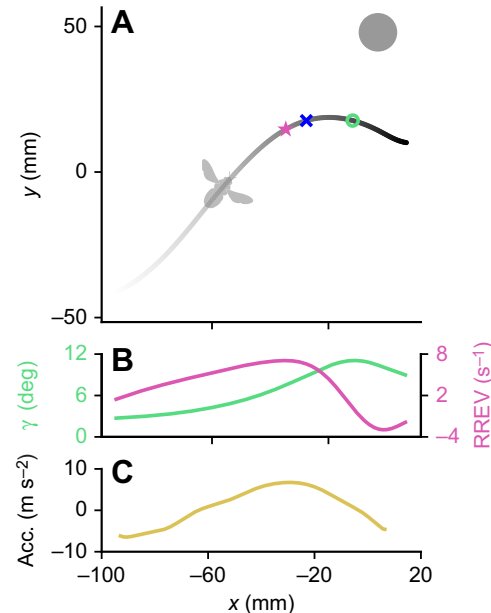

Fig. 5. Obstacle approach. (A) Sample section of a trajectory showing a bee approaching an obstacle and deviating away. (B) Angle subtended by the obstacle on the bee's retina (γ) and the relative retinal expansion velocity (RREV) during the flight segment. (C) The total acceleration of the bee (Acc.) during the flight segment. In A, the grayscale indicates variation in time along the trajectory, the star indicates the location of maximum RREV, the circle indicates the location of the maximum rate of optical expansion of the obstacle ($\dot{\gamma}_{max}$) and the cross indicates the location of the maximum retinal size of the obstacle (γ_{max}). Comparing A–C, as the bee approaches the obstacle, maximum RREV occurs earlier in the trajectory and coincides with maximum acceleration.
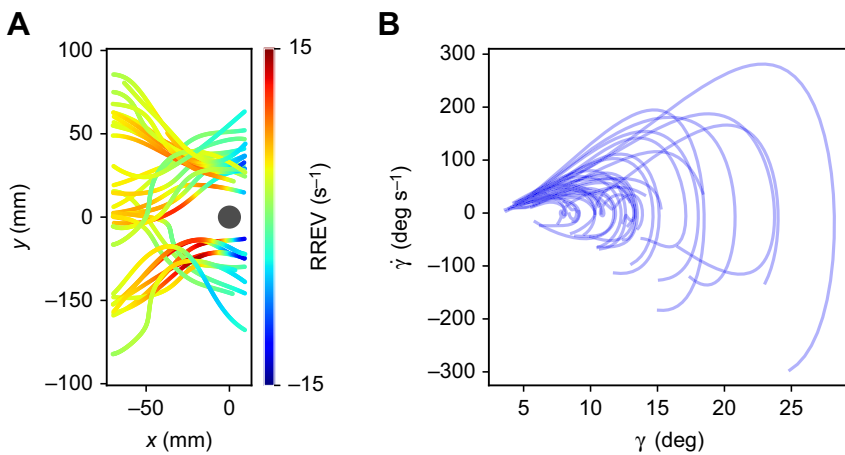
Fig. 6. Flight-path deviation. (A) Flight segments, plotted relative to obstacle location, where the bees approached an obstacle and deviated away to avoid imminent collisions. The colourmap on each trajectory indicates the magnitude of RREV at that instant. (B) The time-resolved variation in the angle subtended by the obstacle on the retina (γ) versus the optical expansion of the obstacle ($\dot{\gamma}$) for segments of flights plotted in A. As bees approached the obstacle and successfully avoided collision, both $\dot{\gamma}$ and γ tended to increase followed by a rapid reduction.

evasion stages of the bees relative to the obstacle (Fig. 6A). Examining the time course of the bees' acceleration and the RREV revealed that RREV$_{max}$ appears to coincide with the maximum in the bees' acceleration (Fig. 5B,C). For the flight segments where imminent collisions were averted, RREV$_{max}$ and the magnitude of acceleration at that instant displayed a strong positive relationship (R^2=0.749, regression slope=0.7024; see Fig. 7C).

The maximum angular acceleration (torque) is putatively considered as an indicator for the onset of the evasive reaction in insects; however, accurately estimating rotational acceleration was difficult in our free-flight experiment because of the noise introduced by double-differentiating the time course of the bees' thorax orientation. Furthermore, under the naturally closed-loop and free-flight conditions here, no distinct 'decision point' was observable to signify evasion onset. Instead, the rate of change in RREV was used to estimate the onset of evasion. For the flight segments where imminent collisions were averted, as bees approached an obstacle, the RREV would increase, followed by a reduction. The instance where the rate of change in RREV became negative was noted to signify evasion initiation (Fig. 8A). While there were some variations between the different flight segments, bees nominally commenced evasion when the RREV was around 5.22 s^{-1}, or 192 ms before collision (see Fig. 8B).

Finally, to unravel the dynamics of the obstacle-avoidance manoeuvres, the thorax acceleration of bees in a TCS was analysed when RREV was maximum, and is presented as a rose histogram (see Fig. 9A). The acceleration of the bees at RREV$_{max}$ was mainly oriented laterally and in some cases with small longitudinal components. Bees' lateral acceleration appeared to be closely

related to their thorax roll angle with a regression slope of 7.88±1.08 m s^{-2} rad^{-1} (mean±s.d., n=15) (see Fig. 9B).

DISCUSSION
Head–thorax coordination and obstacle detection
Bumblebees in our experiment maintained collision-free flight even in their first attempt through the obstacle course. While manoeuvring between the obstacles, bees stabilized the roll angle of their head with respect to their surroundings by implementing rotations counter to the thorax rotation (Fig. 1B; Movie 2). Other insects, such as flies and honeybees, were also found to stabilize the roll angle of their head during aerial manoeuvres in other behavioural contexts by performing a corresponding counter-roll with respect to the thorax (Boeddeker and Hemmi, 2010; Hateren and Schilstra, 1999; Hengstenberg, 1988). Wasps and hawkmoths in tethered preparations have also been shown to modulate their head roll orientation to minimize wide-field rotations along the roll axis (Viollet and Zeil, 2013; Windsor and Taylor, 2017). Here, we note that head stabilization in insects extends to pitch rotations as well (Fig. 1B), though pitch variations of the thorax (and head) were generally much lower compared with roll and yaw. Bumblebees also stabilized their head along the yaw axis whereas major yaw rotations occurred during saccades (Figs 1 and 2), similar to the active flight and gaze strategies observed in flies and wasps during flight in unobstructed terrain (Egelhaaf et al., 2010; Hateren and Schilstra, 1999; Voss and Zeil, 1998).

What is the significance of this strategy for spatial vision, in the context of flight through cluttered environments? Comparison between the yaw orientation of the head and the flight paths
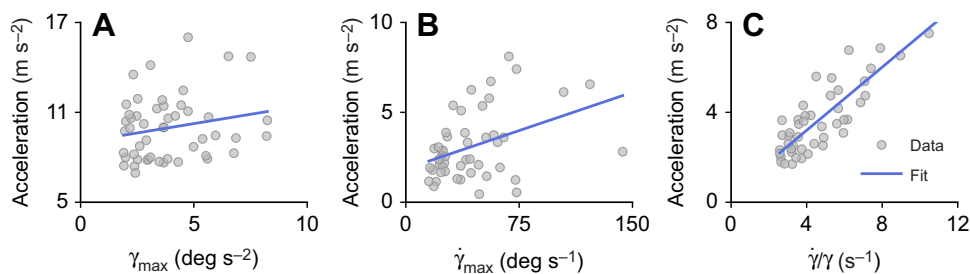

Fig. 7. Collision avoidance. (A) Scatter plot between the maximum angle subtended by the obstacle (γ_{max}) for segments of flights where the bees approached an obstacle and deviated away, avoiding imminent collisions, and the bees' absolute acceleration at the respective instances (n=48, fit equation y=0.2491x+9.001, R^2=0.0208 and slope P=0.159). (B) Scatter plot of the maximum rate of optical expansion of the obstacle ($\dot{\gamma}_{max}$; n=48, fit equation y=0.0283x+1.855, R^2=0.145 and slope P=0.0044) and the bees' absolute acceleration at the respective instances. (C) Scatter plot between maximum RREV of the obstacle and the bees' absolute acceleration at the respective instances (n=48, fit equation y=0.7024x+0.390, R^2=0.749 and slope P<10^{-4}). Comparing the goodness of fit for A–C, the evasive acceleration most closely matches maximum RREV.
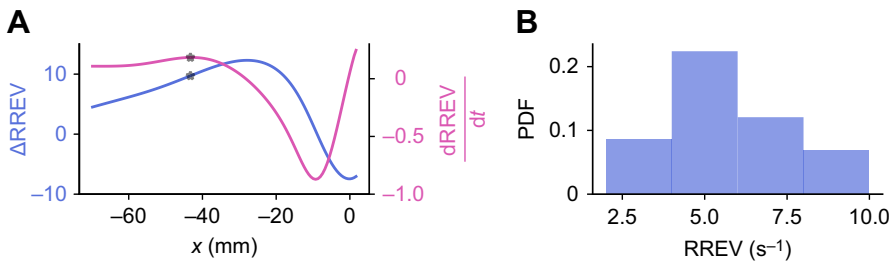
Fig. 8. Initiation of evasion. (A) Variation in RREV and the rate of change of RREV of a sample flight from Fig. 5A, where the bee approached an obstacle and avoided imminent collision. The star marks the point where the slope of the rate of change of RREV was zero and tended towards negative, taken to be the onset of evasion. (B) PDF of the RREV at evasion onset for all flight segments ($n=48$) where the bees avoided collisions.

indicates that bees navigating between obstacles appeared to maintain close alignment between their gaze and the direction of motion (Fig. 3B,C). Such alignment would result in obstacles in a collision course appearing in the frontal visual field where bumblebees and other insects have their highest visual acuity (Taylor et al., 2019). This approach will be useful during flight in natural environments where unexpected obstacles may occur along the flight path. Furthermore, using the frontal section of the visual field for obstacle detection would permit insects to employ vision and optic flow in other retinal regions for other navigational tasks such as odometry and altitude stabilization, respectively (Baird et al., 2021; Kern et al., 2012; Srinivasan, 2020). Measurements made on the head and body orientation of tethered fruit flies, that were capable of freely yawing, have also revealed similar behaviour where (re)alignment between the head and body is achieved through rapid head saccades (Cellini et al., 2021).

Comparison between the optic flow profiles generated using the trajectory and orientation of the bees' thorax and head, respectively, highlights the significance of gaze stabilization on spatial perception and the capacity to detect obstacles (Fig. 4; Movie 3). The optic flow evaluated from the bees' thorax data would be unsuitable for navigation as it was affected by the large rotations, resulting in poor fidelity with the spatial profile of the environment. Such a situation would arise if the head and thorax were rigidly connected or if the eyes were located on the thorax. In contrast, head stabilization performed by the bees during intersaccades resulted in optic flow that reflected the spatial profile of the environment and features critical for navigation, such as the side walls and floor of the tunnel. Gaze stabilization also created high motion contrast between close objects and their background, facilitating obstacle detection (Fig. 4E). Previous studies have suggested that insects perceive the differences between the foreground and background from variation in optic flow and may use motion contrast for depth estimation and object detection (Dittmar et al., 2010; Ravi et al., 2019; Voss and Zeil, 1998; Werner et al., 2016). Unlike the flight ahead of a solitary gap where bumblebees perform extensive lateral peering

manoeuvres to perceive the affordance of passability (Ravi et al., 2020), no such manoeuvring was noted ahead of the obstacles here. This could be because the environment presented here contained slender obstacles with relatively large gaps (>70 mm) between them.

Obstacle avoidance
As optic flow does not contain information on the absolute distance to obstacles, how do bees anticipate and avert collisions? The relationship between the instantaneous acceleration of the bees during intersaccadic flight segments and visual variables was examined to uncover the cues that may have guided the bees' behaviour (Figs 5 and 6A). Such an approach is warranted because during natural free flight through clutter – unlike, for example, landing manoeuvres where behavioural markers such as leg extension can be noted (Lin et al., 2014; Liu et al., 2019; Wagner, 1982) – no discreet behavioural indicators or decision points may be obvious.

Comparing the time course of the retinal size of the obstacle with the bees' acceleration suggested that retinal size may not have a considerable influence on the bees' flight dynamics (Figs 5 and 7A), possibly because the retinal size cannot be used to distinguish between an obstacle's size and distance to its location. A large obstacle further away and a small obstacle located close by will subtend a similar retinal size. Moreover, on many occasions, the bees flew close to the obstacles without performing massive evasion (Fig. 6A), during which time the obstacle would have subtended a large angle, suggesting that it is unlikely that the bees were steering based on a threshold of γ. Similarly, the rate of optical expansion of the obstacle also did not seem to affect the bees' steering (Fig. 7B). One possible explanation could be that the rate of optical expansion only accounts for the approach speed and not the distance to the obstacle, i.e. a faster approach towards an obstacle can be maintained when the obstacle is further away, resulting in the same retinal expansion velocity. However, these parameters are used by insects to guide flight in some behavioural contexts. Flies escaping a visual stimulus or during the later stages of landing
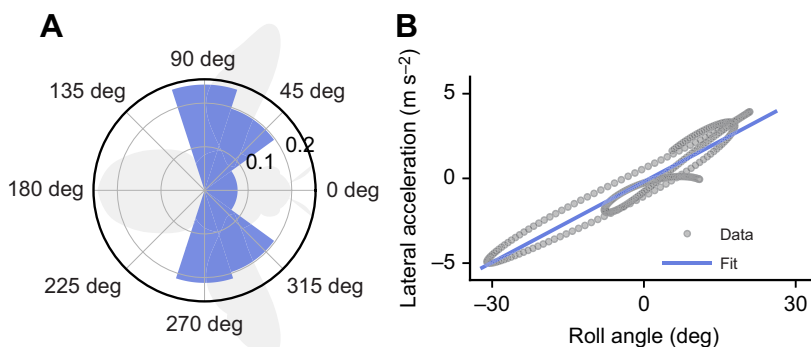

Fig. 9. Dynamics of obstacle-avoidance manoeuvres. (A) Rose histogram of the acceleration direction of the bees when RREV was maximum ($n=15$) showing that the evasive accelerations were orientated laterally. (B) Scatter plot of the time course of the bees' thorax roll angle versus its lateral acceleration for a sample flight trajectory through the obstacle course ($n=319$, fit equation $y=0.166x-0.196$, $R^2=0.916$ and slope $P<10^{-4}$). The close fit in B suggests that the bees produced lateral accelerations for avoiding imminent collision by modulating the roll of their thorax.

modulate their response based on a threshold of retinal size (Fotowat et al., 2009; van Breugel and Dickinson, 2012), whereas honeybees seeking to land on a designated target tend to maintain constant optic flow during their final approach phase. The differences in these strategies compared with those of bumblebees flying through the obstacle course may be due to differences in the behavioural paradigms. Unlike collision avoidance, landing requires a smooth reduction in flight speed until touch-down, enabled by maintaining the retinal expansion or optic flow rate at a constant value (see Baird et al., 2013). For flight through cluttered environments, no such boundary condition exists as all trajectories that do not result in a collision can be considered equally successful.

During the intersaccade segments where bees approached obstacles and avoided imminent collision, a close match between the RREV and the bees' evasive acceleration was noted (Figs 5C and 7C). Bees implemented greater evasion as RREV of an obstacle in the collision course increased. The dimension of RREV is s^{-1} and it can be considered as the inverse of time to contact or collision (TTC) (Lee, 1976), a term commonly used in the context of navigation of robots (Souhila and Karim, 2007) and vertebrates (Yan et al., 2011). The close association between RREV and evasive acceleration noted here does not suggest that bees actively evaluated the time before collision or that their behaviour displayed 'perception of time'. Instead, the TTC may be an implicit result of evaluating RREV from visual information. The relationship between the time course of the bee's acceleration and RREV was also used to estimate the evasion onset that occurred when the bees were around $5.2\ s^{-1}$ from the obstacle (Fig. 8). This translates to around 200 ms, which is well within the range of sensorimotor response times for flying insects.

Other studies have also alluded to insects and birds using RREV (or TTC) in guiding flight tasks, such as flies landing on a vertical post (Balebail et al., 2019; van Breugel and Dickinson, 2012; Wagner, 1982), landing upside-down on the ceiling (Liu et al., 2019) or navigating a chicane (Kern et al., 2012), and pigeons avoiding looming objects (Wang and Frost, 1992). Indeed, one of the requirements for controlling flight using such cues is the ability to parse the visual information to effectively identify obstacles and evaluate metrics such as RREV. The RREV could, for example, be derived from optic flow, because the geometric optic flow derived from pure translation is related to the TTC. We highlighted that the optic flow as seen from the thorax motion represents not so much the spatial surroundings as the optic flow perceived by the bee, thanks to the bee actively controlling its head (Figs 2 and 4). Thus, the stabilized head probably aids in providing visual information for evaluating RREV. Electrophysiological evidence for RREV estimation in birds has been reported in Wang and Frost (1992), while neurons that respond to the retinal size of looming objects have been reported in locusts (Fotowat and Gabbiani, 2011). Further research is needed to verify the neural basis for estimation of RREV in insects such as bees.

Evasion

The final stage of avoiding crashing into an obstacle involves flight manoeuvres that lead to deviation from a collision course. The rose histogram of the bee acceleration when RREV was maximum indicates that evasion was achieved by accelerating laterally (Fig. 9A). The time course of thorax roll angle was linearly related to lateral acceleration (Fig. 9B), the slope of which matches theoretical predictions based on helicopter theory and those reported in previous studies (e.g. Ravi et al., 2016). Thus, bees produced lateral accelerations for avoiding imminent collision by

modulating roll of their thorax. This is further supported by the largest rotations of the thorax noted in the roll axis as compared with the pitch and yaw axes (Fig. 2C). Unlike fruit flies, which execute rapid evasive manoeuvres by simultaneously rolling and pitching (Muijres et al., 2014), bees did not significantly decelerate their flight speed and alter thorax pitch as they encountered obstacles. As the bees were flying through a familiar tunnel and encountered relatively small (unfamiliar) obstacles, the manoeuvres performed were not extreme evasion sequences where strategies may be different. Though bees could change flight path by, in theory, varying either the yaw or roll orientation of their thorax (thrust vectoring), rolling represents an energetically efficient means of manoeuvring, as rotations occur around the axis of least inertia. Increasing evidence suggests that using roll to manoeuvre is a common strategy among many flying animals (Muijres et al., 2014; Ros et al., 2011; Schilstra and van Hateren, 1998).

Conclusions

To support behaviour, an animal relies upon its sensorimotor system, which is probably tuned to both its own physiology and its habitat. We found that during flight through cluttered environments, bees displayed all the characteristics of active vision including stabilizing head roll and pitch orientation with respect to their environment, while yaw rotations mainly occurred during saccades. Bees aligned their head with the direction of motion, which ensured that the bee (head and then thorax) was oriented toward openings, and any obstacles in the collision course mainly appeared in the frontal part of the visual field.

When bees avoided imminent collisions, the $RREV_{max}$ was closely related to the magnitude of evasion acceleration, suggesting that bees may modulate their steering response based on the RREV of the obstacles. Bees avoided crashes by veering laterally through varying their thorax roll angle. This strategy represents an energetically efficient mechanism to introduce deviations to the flight path. Thus, using a concert of sensory and motor control strategies, bees achieve robust flight through unfamiliar and complex environments. Further experiments including electrophysiological recordings as well as dynamic manipulation of obstacle size and position are needed to further test the behavioural significance and neural basis of RREV and other relevant visual cues.

Author contributions
Conceptualization: S.R., T.S., A.F., M.E.; Methodology: S.R., T.S.; Formal analysis: S.R., O.J.B., L.L., C.D., A.F., W.H.W., M.E.; Investigation: S.R., T.S.; Writing - original draft: S.R., O.J.B., L.L., C.D., A.F., W.H.W., M.E.; Writing - review & editing: S.R., O.J.B., L.L., C.D., A.F., W.H.W., M.E.; Visualization: S.R., L.L., C.D., A.F.; Supervision: S.R., M.E.; Funding acquisition: S.R.

References

Baird, E. and Dacke, M. (2012). Visual flight control in naturalistic and artificial environments. *J. Comp. Physiol. A. Neuroethol. Sens. Neural. Behav. Physiol.* **198**, 869-876. doi:10.1007/s00359-012-0757-7

Baird, E., Boeddeker, N., Ibbotson, M. R. and Srinivasan, M. V. (2013). A universal strategy for visually guided landing. *Proc. Natl. Acad. Sci.* **110**, 18686-18691. doi:10.1073/pnas.1314311110

Baird, E., Boeddeker, N. and Srinivasan, M. V. (2021). The effect of optic flow cues on honeybee flight control in wind. *Proc. R. Soc. B Biol. Sci.* **288**, 20203051. doi:10.1098/rspb.2020.3051

Balebail, S., Raja, S. K. and Sane, S. P. (2019). Landing maneuvers of houseflies on vertical and inverted surfaces. *PLoS One* **14**, e0219861. doi:10.1371/journal.pone.0219861

Bertrand, O. J. N., Lindemann, J. P. and Egelhaaf, M. (2015). A Bio-inspired Collision Avoidance Model Based on Spatial Information Derived from Motion Detectors Leads to Common Routes. *PLOS Comput. Biol.* **11**, e1004339. doi:10.1371/journal.pcbi.1004339

Boeddeker, N. and Hemmi, J. M. (2010). Visual gaze control during peering flight manoeuvres in honeybees. *Proceedings. Biol. Sci.* **277**, 1209-1217.

Burnett, N. P., Badger, M. A. and Combes, S. A. (2020). Wind and obstacle motion affect honeybee flight strategies in cluttered environments. *J. Exp. Biol.* **223**, jeb222471. doi:10.1242/jeb.222471

Cellini, B. and Mongeau, J.-M. (2020). Active vision shapes and coordinates flight motor responses in flies. *Proc. Natl. Acad. Sci.* **117**, 23085-23095. doi:10.1073/pnas.1920846117

Cellini, B., Salem, W. and Mongeau, J.-M. (2021). Mechanisms of punctuated vision in fly flight. *Curr. Biol.* **31**, 4009-4024.e3. doi:10.1016/j.cub.2021.06.080

Crall, J. D., Ravi, S., Mountcastle, A. M. and Combes, S. A. (2015). Bumblebee flight performance in cluttered environments: effects of obstacle orientation, body size and acceleration. *J. Exp. Biol.* **218**, 2728-2737. doi:10.1242/jeb.121293

Dittmar, L., Stürzl, W., Baird, E., Boeddeker, N. and Egelhaaf, M. (2010). Goal seeking in honeybees: matching of optic flow snapshots? *J. Exp. Biol.* **213**, 2913-2923. doi:10.1242/jeb.043737

Doussot, C., Bertrand, O. J. N. and Egelhaaf, M. (2021). The critical role of head movements for spatial representation during bumblebees learning flight. *Front. Behav. Neurosci.* **14**. doi:10.3389/fnbeh.2020.606590

Dudley, R. (2002). *The Biomechanics of Insect Flight: Form, Function, Evolution.* Princeton University Press.

Egelhaaf, M., Kern, R., Lindemann, J. P., Braun, E. and Geurten, B. (2010). Active vision in blowflies: strategies and mechanisms of spatial orientation. In *Flying Insects and Robots*, pp. 51-61. Springer.

Egelhaaf, M., Boeddeker, N., Kern, R., Kurtz, R. and Lindemann, J. P. (2012). Spatial vision in insects is facilitated by shaping the dynamics of visual input through behavioral action. *Front. Neural Circuits* **6**, 108. doi:10.3389/fncir.2012.00108

Egelhaaf, M., Kern, R. and Lindemann, J. P. (2014). Motion as a source of environmental information: a fresh view on biological motion computation by insect brains. *Front. Neural Circuits* **8**, 127. doi:10.3389/fncir.2014.00127

Foster, D. J. and Cartar, R. V. (2011). What causes wing wear in foraging bumble bees? *J. Exp. Biol.* **214**, 1896-1901. doi:10.1242/jeb.051730

Fotowat, H. and Gabbiani, F. (2011). Collision detection as a model for sensory-motor integration. *Annu. Rev. Neurosci.* **34**, 1-19. doi:10.1146/annurev-neuro-061010-113632

Fotowat, H., Fayyazuddin, A., Bellen, H. J. and Gabbiani, F. (2009). A novel neuronal pathway for visually guided escape in Drosophila melanogaster. *J. Neurophysiol.* **102**, 875-885. doi:10.1152/jn.00073.2009

Hateren, J. and Schilstra, C. (1999). Blowfly flight and optic flow. II. Head movements during flight. *J. Exp. Biol.* **202**, 1491-1500.

Hedrick, T. L. (2008). Software techniques for two- and three-dimensional kinematic measurements of biological and biomimetic systems. *Bioinspir. Biomim.* **3**, 034001.

Hengstenberg, R. (1988). Mechanosensory control of compensatory head roll during flight in the blowflyCalliphora erythrocephala Meig. *J. Comp. Physiol. A* **163**, 151-165. doi:10.1007/BF00612425

Kern, R., Boeddeker, N., Dittmar, L. and Egelhaaf, M. (2012). Blowfly flight characteristics are shaped by environmental features and controlled by optic flow information. *J. Exp. Biol.* **215**, 2501-2514. doi:10.1242/jeb.061713

Lecoeur, J., Dacke, M., Floreano, D. and Baird, E. (2019). The role of optic flow pooling in insect flight control in cluttered environments. *Sci. Rep.* **9**, 1-13. doi:10.1038/s41598-019-44187-2

Lee, D. N. (1976). A Theory of Visual Control of Braking Based on Information about Time-to-Collision. *Perception* **5**, 437-459. doi:10.1068/p050437

Lin, H.-T., Ros, I. G. and Biewener, A. A. (2014). Through the eyes of a bird: modelling visually guided obstacle flight. *J. R. Soc. Interface* **11**, 20140239. doi:10.1098/rsif.2014.0239

Liu, P., Sane, S. P., Mongeau, J.-M., Zhao, J. and Cheng, B. (2019). Flies land upside down on a ceiling using rapid visually mediated rotational maneuvers. *Sci. Adv.* **5**, eaax1877. doi:10.1126/sciadv.aax1877

Mauss, A. S. and Borst, A. (2020). Optic flow-based course control in insects. *Curr. Opin. Neurobiol.* **60**, 21-27. doi:10.1016/j.conb.2019.10.007

Mountcastle, A. M., Alexander, T. M., Switzer, C. M. and Combes, S. A. (2016). Wing wear reduces bumblebee flight performance in a dynamic obstacle course. *Biol. Lett.* **12**, 20160294. doi:10.1098/rsbl.2016.0294

Muijres, F. T., Elzinga, M. J., Melis, J. M. and Dickinson, M. H. (2014). Flies evade looming targets by executing rapid visually directed banked turns. *Science* **344**, 172-177. doi:10.1126/science.1248955

Nityananda, V. and Read, J. C. A. (2017). Stereopsis in animals: evolution, function and mechanisms. *J. Exp. Biol.* **220**, 2502-2512. doi:10.1242/jeb.143883

Odenthal, L., Doussot, C., Meyer, S. and Bertrand, O. J. N. (2021). Analysing head-thorax choreography during free-flights in bumblebees. *Front. Behav. Neurosci.* **14**, 610029. doi:10.3389/fnbeh.2020.610029

Osborne, J. L., Martin, A. P., Carreck, N. L., Swain, J. L., Knight, M. E., Goulson, D., Hale, R. J. and Sanderson, R. A. (2008). Bumblebee flight distances in relation to the forage landscape. *J. Anim. Ecol.* **77**, 406-415. doi:10.1111/j.1365-2656.2007.01333.x

Ravi, S., Kolomenskiy, D., Engels, T., Schneider, K., Wang, C., Sesterhenn, J. and Liu, H. (2016). Bumblebees minimize control challenges by combining active and passive modes in unsteady winds. *Sci. Rep.* **6**, 35043. doi:10.1038/srep35043

Ravi, S., Bertrand, O., Siesenop, T., Manz, L.-S., Doussot, C., Fisher, A. and Egelhaaf, M. (2019). Gap perception in bumblebees. *J. Exp. Biol.* **222**, jeb184135. doi:10.1242/jeb.184135

Ravi, S., Siesenop, T., Bertrand, O., Li, L., Doussot, C., Warren, W. H., Combes, S. A. and Egelhaaf, M. (2020). Bumblebees perceive the spatial layout of their environment in relation to their body size and form to minimize inflight collisions. *Proc. Natl. Acad. Sci.* **117**, 31494-31499. doi:10.1073/pnas.2016872117

Riabinina, O., de Ibarra, N. H., Philippides, A. and Collett, T. S. (2014). Head movements and the optic flow generated during the learning flights of bumblebees. *J. Exp. Biol.* **217**, 2633-2642. doi:10.1242/jeb.102897

Ros, I. G., Bassman, L. C., Badger, M. A., Pierson, A. N. and Biewener, A. A. (2011). Pigeons steer like helicopters and generate down- and upstroke lift during low speed turns. *Proc. Natl. Acad. Sci. U. S. A.* **108**, 19990-19995. doi:10.1073/pnas.1107519108

Schilstra, C. and van Hateren, J. H. (1998). Stabilizing gaze in flying blowflies. *Nature* **395**, 654-654. doi:10.1038/27114

Serres, J. R. and Ruffier, F. (2017). Optic flow-based collision-free strategies: From insects to robots. *Arthropod Struct. Dev.* **46**, 703-717. doi:10.1016/j.asd.2017.06.003

Shoemaker, P. A., Hyslop, A. M. and Humbert, J. S. (2011). Optic flow estimation on trajectories generated by bio-inspired closed-loop flight. *Biol. Cybern.* **104**, 339-350. doi:10.1007/s00422-011-0436-8

Souhila, K. and Karim, A. (2007). Optical flow based robot obstacle avoidance. *Int. J. Adv. Robot. Syst.* **4**, 2. doi:10.5772/5715

Srinivasan, M. V. (2020). Vision, perception, navigation and 'cognition' in honeybees and applications to aerial robotics. *Biochem. Biophys. Res. Commun.* **564**, 4-17. doi:10.1016/j.bbrc.2020.09.052

Taylor, G. J., Tichit, P., Schmidt, M. D., Bodey, A. J., Rau, C. and Baird, E. (2019). Bumblebee visual allometry results in locally improved resolution and globally improved sensitivity. *Elife* **8**, 1-32. doi:10.7554/eLife.40613

van Breugel, F. and Dickinson, M. H. (2012). The visual control of landing and obstacle avoidance in the fruit fly Drosophila melanogaster. *J. Exp. Biol.* **215**, 1783-1798. doi:10.1242/jeb.066498

Viollet, S. and Zeil, J. (2013). Feed-forward and visual feedback control of head roll orientation in wasps (Polistes humilis, Vespidae, Hymenoptera). *J. Exp. Biol.* **216**, 1280-1291. doi:10.1242/jeb.074773

Voss, R. and Zeil, J. (1998). Active vision in insects: an analysis of object-directed zig-zag flights in wasps (Odynerus spinipes ?, Eumenidae). *J. Comp. Physiol. A Sensory, Neural, Behav. Physiol.* **182**, 377-387. doi:10.1007/s003590050187

Wagner, H. (1982). Flow-field variables trigger landing in flies. *Nature* **297**, 147-148. doi:10.1038/297147a0

Wang, Y. and Frost, B. J. (1992). Time to collision is signalled by neurons in the nucleus rotundus of pigeons. *Nature* **356**, 236-238. doi:10.1038/356236a0

Werner, A., Stürzl, W. and Zanker, J. (2016). Object recognition in flight: how do bees distinguish between 3D shapes? *PLoS One* **11**, e0147106. doi:10.1371/journal.pone.0147106

Windsor, S. P. and Taylor, G. K. (2017). Head movements quadruple the range of speeds encoded by the insect motion vision system in hawkmoths. *Proc. R. Soc. B Biol. Sci.* **284**, 20171622. doi:10.1098/rspb.2017.1622

Yan, J.-J., Lorv, B., Li, H. and Sun, H.-J. (2011). Visual processing of the impending collision of a looming object: Time to collision revisited. *J. Vis.* **11**, 7-7. doi:10.1167/11.12.7

Movie 1. Animation of the experiment setup including a bee with markers on the head and thorax that is flying through the obstacle course.

Movie 2. Two sample highspeed videos of bees flying through the obstacle course
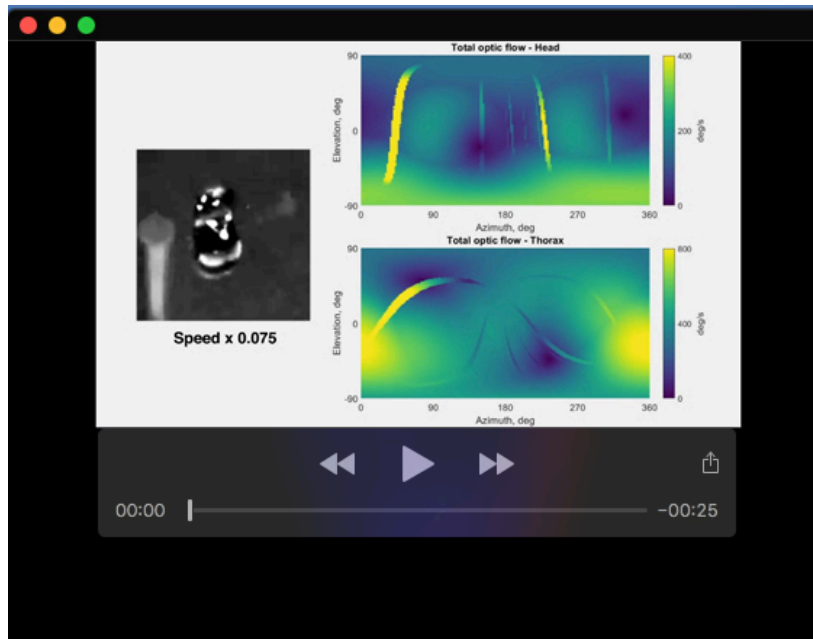
Movie 3. Part I: For Sample 1 flight in SV2, instantaneous heatmaps of the optic flow across the spherical visual field calculated using the bee's head and thorax position and orientation respective. Also included in the video is a zoomed view centred on the bee. Part II: For the same flight instantaneous heatmaps of the nearness map across the spherical visual field calculated using the bee's head and thorax position and orientation respective. Also included in the video is a zoomed view centred on the bee.